J Eng Math (2010) 67:23–32
DOI 10.1007/s10665-009-9323-x

Tsunamis and acoustic-gravity waves from underwater earthquakes

Michael Stiassnie

Received: 29 May 2008 / Accepted: 18 August 2009 / Published online: 16 September 2009

Abstract A study of wave radiation by a piston bottom displacement, in a compressible ocean of constant depth, is carried out within the framework of a two-dimensional linear theory. Simple analytic expressions for the flow field, at a large distance from the disturbance, are derived. A realistic numerical example indicates that the *Acoustic-Gravity* waves, which significantly precede the tsunami, are expected to leave a significant signature on bottom-pressure records that should be considered for early detection of tsunamis.

Keywords Compressible ocean · Surface waves · Tsunami detection

1 Introduction

The 2004 Indian Ocean earthquake was an undersea earthquake that occurred at 00:58:53 UTC December 26, 2004, with an epicenter off the west coast of Sumatra, Indonesia. The earthquake triggered a series of devastating tsunamis along the coasts of most landmasses bordering the Indian Ocean, killing more than 225,000 people in 11 countries, and inundating coastal communities with waves up to 30 m. It was one of the deadliest natural disasters in history. Indonesia, Sri Lanka, India, and Thailand were hardest hit.

The plight of the many affected people and countries prompted a widespread humanitarian response. In all, the world-wide community donated more than $7 billion in humanitarian aid.

This tsunami, like all others, behaved very differently in deep water than in shallow water. In deep ocean water, tsunami waves form only a small hump, barely noticeable and harmless, which generally travels at a very high speed of 500–1,000 km/h. In shallow water near coastlines, a tsunami slows down to only tens of kilometers an hour, but in doing so, forms large destructive waves. Scientists investigating the damage in Aceh found evidence that the wave reached a height of 24 m when coming ashore along large stretches of the coastline, rising to 30 m in some areas when traveling inland.

Radar satellites recorded the heights of tsunami waves in deep water: at 2 h after the earthquake, the maximum height was 60 cm. These are the first such observations ever made. However, these observations could not have been used to provide a warning, because the satellites were not intended for that purpose and the data took hours

M. Stiassnie (✉)
Faculty of Civil and Environmental Engineering,
Technion-Israel Institute of Technology, 32000 Haifa, Israel
e-mail: miky@tx.technion.ac.il

to analyze. Due to the distances involved, the tsunami took anywhere from 15 min to 7 h (for Somalia) to reach the various coastlines. The tsunami was observed as far as Struisbaai in South Africa, a distance of 8,500 km, where a 1.5 m high wave surged on shore about 16 h after the earthquake had occurred. Despite a lag of up to several hours between the earthquake and the impact of the tsunami, nearly all of the victims were taken completely by surprise. There were no tsunami warning systems in the Indian Ocean to detect tsunamis or to warn the population living around the ocean vicinity. Tsunami detection is difficult: as a tsunami occurs in deep water, it has little height, and a network of sensors is needed to detect it. Setting up the communications infrastructure to issue timely warnings is another big problem, particularly in a relatively deprived part of the world.

Ever since this catastrophic event, I have asked myself if there is anything that the science of water waves can contribute to enable more accurate, and in particular, significantly earlier tsunami warnings. The current article is a first outcome of this quest.

In a series of recent studies, the Russian group lead by Prof. M.A. Nosov, has demonstrated the importance of the small compressibility of the ocean in the process of tsunami generation [1–5]. These studies follow the foundation laid in earlier attempts by Miyoshi [6], Sells [7], and Yamamoto [8]; see also [9].

The overwhelming majority of ocean-wave studies ignore the minute compressibility of the water, which is expected to have, and in most cases has, only a negligible effect on the main physical processes. However, a rather straightforward analysis of the linearized problem in water of constant depth reveals that for any wave period (T) smaller than four times the water depth (h) to the speed of sound (c) ratio (i.e., $T < 4h/c$); two or more propagating modes are possible.

This state-of-affairs is rather different from the situation in an incompressible ocean, for which only one propagating mode exists. In the balance of this paper, we shall refer to these modes by their wave-numbers: $k_o > 2\pi/cT > k_1 > k_2 > \cdots > k_N$; where k_o represents the mode which also exists in an incompressible ocean, and will be called the tsunami mode, whereas $k_1, k_2, \ldots, k_N$, represent the additional propagating modes, which result from taking the compressibility of the water into account, and will be called the *Acoustic-Gravity*[1] modes. A disturbance at the ocean floor, such as caused by a submarine earthquake, produces many different modes. Most of these modes ($k_{N+1}, k_{N+2}\ldots$) are non-propagating (evanescent), and of local importance only. However, the tsunami (k_o), and the leading *Acoustic-Gravity* mode k_1 (and of less importance also $k_2, \ldots, k_N$), propagate away from the earthquake site, and travel to a great distance. The *Acoustic-Gravity* wave travels significantly faster than the tsunami, and thus, is a possible candidate for an early warning about the approach of the latter.

The main results of this article are: (i) providing an analytical solution for the *Acoustic-Gravity* modes at large distance from the disturbance (i.e., from the earthquake epicenter); and (ii) providing numerical values for the free-surface elevation and for the dynamic bottom pressure, generated by the *Acoustic-Gravity* waves, in order to enable an assessment of their experimental detectability.

The present study is limited to a two-dimensional configuration, to constant water-depth, and neglects dissipation; these constraints must be relaxed in future investigations. The mathematical problem is formulated in Sect. 2, and solved in Sect. 3. Asymptotic results for large distance are given in Sect. 4; and an illustrative numerical example is provided in Sect. 5. Concluding remarks are drawn in Sect. 6.

2 Formulation

Let us consider a layer of an ideal compressible homogeneous fluid of constant depth h in the field of gravity, and assume that it is unbounded in the horizontal x-direction. The origin of the Cartesian coordinate system oxy is at the unperturbed bottom, and the y-axis is oriented upwards. In order to find the wave disturbance $y = h + \eta(x, t)$ that is excited at the fluid surface by a bottom motion $y = \zeta(x, t)$, it is necessary to solve for the flow velocity potential $\varphi(x, y, t)$ which is governed by the wave-equation

[1] Some authors refer to these waves as hydro-acoustic waves and classify them as part of the T-phase phenomenon.

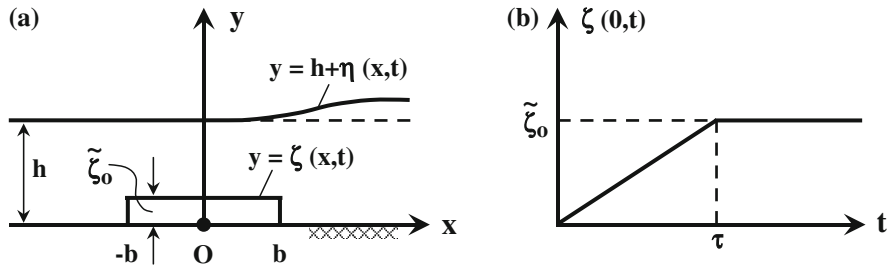

Fig. 1 **a** Flow domain, **b** bottom motion

$$\varphi_{xx} + \varphi_{yy} = \frac{1}{c^2}\varphi_{tt}, \quad 0 \le y \le h \tag{2.1}$$

and the linearized free-surface and bottom boundary conditions:

$$\varphi_{tt} + g\varphi_y = 0, \quad y = h, \tag{2.2}$$

$$\varphi_y = \zeta_t, \quad y = 0, \tag{2.3}$$

where c is the speed of sound in the water, and g is the acceleration due to gravity. Note that besides the motion ζ the bottom is assumed to be rigid.

The free-surface elevation and the dynamic bottom pressure are given, respectively, by:

$$\eta = -\frac{1}{g}\varphi_t, \quad y = h \tag{2.4}$$

and

$$p_b = -\rho\varphi_t, \quad y = 0, \tag{2.5}$$

where ρ is the water density.

The chosen disturbance of the bottom is described in Fig. 1 and by

$$\zeta_t(x,t) = \frac{\tilde{\zeta}_o}{\tau} H\left(b^2 - x^2\right) H\left(t\left(\tau - t\right)\right), \tag{2.6}$$

where H is the Heaviside function; $\tilde{\zeta}_o$, b are the geometrical characteristics of the earthquake and τ is its duration.

3 Solution

The $t \to \omega$ Fourier transform of the velocity potential is defined by

$$f(x,y,\omega) = \frac{1}{\sqrt{2\pi}} \int_{-\infty}^{\infty} \varphi(x,y,t)\, \mathrm{e}^{-\mathrm{i}\omega t}\mathrm{d}t \tag{3.1}$$

Substituting (2.6) in (2.3) and taking the Fourier transform of (2.1), (2.2) and (2.3) yields

$$f_{xx} + f_{yy} = -\frac{\omega^2}{c^2} f, \quad 0 \le y \le h, \tag{3.2}$$

$$f_y - \frac{\omega^2}{g} f = 0, \quad y = h, \tag{3.3}$$

$$f_y = \zeta_o(\omega) H\left(b^2 - x^2\right), \quad y = 0, \tag{3.4a}$$

where

$$\zeta_o(\omega) = \frac{\mathrm{i}\tilde{\xi}_o}{\sqrt{2\pi}} \frac{\left(\mathrm{e}^{-\mathrm{i}\omega\tau} - 1\right)}{\omega\tau}. \tag{3.4b}$$

Yamamoto [8] has studied a related problem in which the disturbed bottom-block, $x \in (-b, b)$, oscillates periodically with frequency ω. Yamamoto has reached the same mathematical problem as our (3.2), (3.3) and (3.4), which he solved by applying a Fourier-transform over the horizontal axis x.

From the results of Yamamoto, the solution of (3.2)–(3.4) is obtained as

$$\begin{aligned} f(x,y,\omega) = 4\zeta_o(\omega) \Bigg\{ & \frac{c\left[\cos\left(\omega(y-h)/c\right) + (\omega c/g)\cdot\sin\left(\omega(y-h)/c\right)\right]}{4\omega\left[\sin(\omega h/c) + (\omega c/g)\cos(\omega h/c)\right]} \\ & - \frac{\mu_o \mathrm{e}^{-\mathrm{i}\,\mathrm{sign}(\omega)k_o b}\cosh(\mu_o y)\cos(k_o x)}{k_o^2\left[2\mu_o h + \sinh(2\mu_o h)\right]} \\ & - \sum_{n=1}^{N} \frac{\mu_n \mathrm{e}^{-\mathrm{i}\,\mathrm{sign}(\omega)k_n b}\cos(\mu_n y)\cos(k_n x)}{k_n^2\left[2\mu_n h + \sin(2\mu_n h)\right]} \\ & + \sum_{n=N+1}^{\infty} \frac{\mu_n \mathrm{e}^{-\lambda_n b}\cos(\mu_n y)\cosh(\lambda_n x)}{\lambda_n^2\left[2\mu_n h + \sin(2\mu_n h)\right]} \Bigg\}, \quad \text{for } |x| < b, \end{aligned} \tag{3.5a}$$

$$\begin{aligned} f(x,y,\omega) = 4\zeta_o(\omega) \Bigg\{ & \frac{\mathrm{i}\mu_o \sin\left[\mathrm{sign}(\omega)\,k_o b\right]\cosh(\mu_o y)\,\mathrm{e}^{-\mathrm{i}\,\mathrm{sign}(\omega)k_o|x|}}{k_o^2\left[2\mu_o h + \sinh(2\mu_o h)\right]} \\ & + \sum_{n=1}^{N} \Bigg\{ \frac{\mathrm{i}\mu_n \sin\left[\mathrm{sign}(\omega)\,k_n b\right]\cos(\mu_n y)\,\mathrm{e}^{-\mathrm{i}\,\mathrm{sign}(\omega)k_n|x|}}{k_n^2\left[2\mu_n h + \sin(2\mu_n h)\right]} \\ & - \sum_{n=N+1}^{\infty} \frac{\mu_n \sinh(\lambda_n b)\cos(\mu_n y)\,\mathrm{e}^{-\lambda_n|x|}}{\lambda_n^2\left[2\mu_n h + \sin(2\mu_n h)\right]} \Bigg\}, \quad \text{for } |x| > b. \end{aligned} \tag{3.5b}$$

Here, μ_o, μ_n (real and positive) are the solutions of

$$\omega^2 = g\mu_o \tanh(\mu_o h); \quad \omega^2 = -g\mu_n \tan(\mu_n h), \quad n = 1, 2, \ldots; \tag{3.6a,b}$$

see the solid curves in Fig. 2.

k_o, k_n, λ_n (real and positive) are given by

$$k_o = \left(\mu_o^2 + k_s^2\right)^{1/2}, \tag{3.7a}$$

$$k_n = \left(k_s^2 - \mu_n^2\right)^{1/2}, \quad n = 1, 2, \ldots, N; \; k_s > \mu_N, \tag{3.7b}$$

$$\lambda_n = \left(\mu_n^2 - k_s^2\right)^{1/2}, \quad n = N+1, \ldots; \; k_s < \mu_{N+1} \tag{3.7c}$$

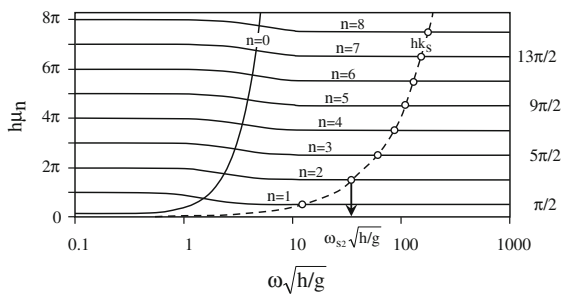

Fig. 2 Solutions of Eq. 3.6a,b ——. Plot of Eq. 3.8 for $h = 4000$ m, and $c = 1500$ m/s - - - - -. Solutions of Eq. 3.11 o, o, o

and

$$k_s = \omega/c. \tag{3.8}$$

The inverse Fourier transform is given by

$$\varphi\,(x,\,y,\,t) = \frac{1}{\sqrt{2\pi}} \int\limits_{-\infty}^{\infty} f\,(x,\,y,\,\omega)\,\mathrm{e}^{\mathrm{i}\omega t}\,\mathrm{d}\omega. \tag{3.9}$$

Substituting (3.5) and (3.4b) in (3.9) gives

$$\begin{aligned}\varphi\,(x,\,y,\,t) = \frac{8\tilde{\zeta}_o}{\pi\,\tau}\Bigg\{ &\int\limits_{o}^{\infty} \frac{c\cdot\sin\,(\omega\tau/2)\,[\cos\,(\omega\,(y-h)\,/c) + (\omega c/g)\sin\,(\omega\,(y-h)\,/c)]}{4\omega^2\,[\sin\,(\omega h/c) + (\omega c/g)\cos\,(\omega h/c)]}\cos\left(\omega t - \frac{\omega\tau}{2}\right)\mathrm{d}\omega \\ &- \int\limits_{o}^{\infty} \frac{\mu_o\sin\,(\omega\tau/2)\cosh\,(\mu_o y)\cos\,(k_o x)}{\omega k_o^2\,[2\mu_o h + \sinh\,(2\mu_o h)]}\cos\left(k_o b - \omega t + \frac{\omega\tau}{2}\right)\mathrm{d}\omega \\ &- \sum_{n=1}^{\infty}\int\limits_{\omega_{sn}}^{\infty} \frac{\mu_n\sin\,(\omega\tau/2)\cos\,(\mu_n y)\cos\,(k_n x)}{\omega k_n^2\,[2\mu_n h + \sin\,(2\mu_n h)]}\cos\left(k_n b - \omega t + \frac{\omega\tau}{2}\right)\mathrm{d}\omega \\ &+ \sum_{n=1}^{\infty}\int\limits_{o}^{\omega_{sn}} \frac{\mu_n\sin\,(\omega\tau/2)\,\mathrm{e}^{-\lambda_n b}\cos\,(\mu_n y)\cosh\,(\lambda_n x)}{\omega\lambda_n^2\,[2\mu_n h + \sin\,(2\mu_n h)]}\cos\left(\omega t - \frac{\omega\tau}{2}\right)\mathrm{d}\omega\Bigg\}, \quad \text{for } |x| < b\end{aligned} \tag{3.10a}$$

$$\begin{aligned}\varphi\,(x,\,y,\,t) = \frac{8\tilde{\zeta}_o}{\pi\,\tau}\Bigg\{ &\int\limits_{o}^{\infty} \frac{\mu_o\sin\,(\omega\tau/2)\sin\,(k_o b)\cosh\,(\mu_o y)}{\omega k_o^2\,[2\mu_o h + \sinh\,(2\mu_o h)]}\sin\left(k_o\,|x| - \omega t + \frac{\omega\tau}{2}\right)\mathrm{d}\omega \\ &+ \sum_{n=1}^{\infty}\int\limits_{\omega_{sn}}^{\infty} \frac{\mu_n\sin\,(\omega\tau/2)\sin\,(k_n b)\cos\,(\mu_n y)}{\omega k_n^2\,[2\mu_n h + \sin\,(2\mu_n h)]}\sin\left(k_n\,|x| - \omega t + \frac{\omega\tau}{2}\right)\mathrm{d}\omega \\ &+ \sum_{n=1}^{\infty}\int\limits_{o}^{\omega_{sn}} \frac{\mu_n\sin\,(\omega\tau/2)\sinh\,(\lambda_n b)\cos\,(\mu_n y)\,\mathrm{e}^{-\lambda_n|x|}}{\omega\lambda_n^2\,[2\mu_n h + \sin\,(2\mu_n h)]}\cos\left(\omega t - \frac{\omega\tau}{2}\right)\mathrm{d}\omega\Bigg\}, \quad \text{for } |x| > b,\end{aligned} \tag{3.10b}$$

where ω_{sn} is given by the root of

$$\mu_n\,(\omega_{sn}) = \omega_{sn}/c, \quad n = 1, 2, \ldots; \tag{3.11}$$

see the small circles in Fig. 2.

A good approximate solution to (3.11) and (3.6b) is

$$\omega_{sn} = \alpha_n c/h,\ \alpha_n = (2n-1)\,\frac{\pi}{2}; \quad n = 1, 2, \ldots. \tag{3.12}$$

From (3.10b) and (2.4), the free surface elevation for $x > b$ is:

$$\begin{aligned}\eta\,(x,\,t) = \frac{8\tilde{\zeta}_o}{\pi g\tau}\Bigg\{ &\int\limits_{o}^{\infty} \frac{\mu_o\sin\,(\omega\tau/2)\sin\,(k_o b)\cosh\,(\mu_o h)}{k_o^2\,[2\mu_o h + \sinh\,(2\mu_o h)]}\cos\left(k_o x - \omega t + \frac{\omega\tau}{2}\right)\mathrm{d}\omega \\ &+ \sum_{n=1}^{\infty}\int\limits_{\omega_{sn}}^{\infty} \frac{\mu_n\sin\,(\omega\tau/2)\sin\,(k_n b)\cos\,(\mu_n h)}{k_n^2\,[2\mu_n h + \sin\,(2\mu_n h)]}\cos\left(k_n x - \omega t + \frac{\omega\tau}{2}\right)\mathrm{d}\omega\end{aligned}$$

$$-\sum_{n=1}^{\infty}\int_{o}^{\omega_{sn}}\frac{\mu_n\sin(\omega\tau/2)\sin(\lambda_n b)\cos(\mu_n h)}{\lambda_n^2\left[2\mu_n h+\sin(2\mu_n h)\right]}\mathrm{e}^{-\lambda_n x}\sin\left(\omega t-\frac{\omega\tau}{2}\right)\mathrm{d}\omega\Bigg\}. \tag{3.13}$$

From (3.10b) and (2.5) the dynamic bottom pressure for $x > b$ is

$$\begin{aligned}P_b(x,t)=\frac{8\rho\tilde{\zeta}_o}{\pi\tau}\Bigg\{&\int_{o}^{\infty}\frac{\mu_o\sin(\omega\tau/2)\sin(k_o b)}{k_o^2\left[2\mu_o h+\sinh(2\mu_o h)\right]}\cos\left(k_o x-\omega t+\frac{\omega\tau}{2}\right)\mathrm{d}\omega\\&+\sum_{n=1}^{\infty}\int_{\omega_{sn}}^{\infty}\frac{\mu_n\sin(\omega\tau/2)\sin(k_n b)}{k_n^2\left[2\mu_n h+\sin(2\mu_n h)\right]}\cos\left(k_n x-\omega t+\frac{\omega\tau}{2}\right)\mathrm{d}\omega\\&-\sum_{n=1}^{\infty}\int_{o}^{\omega_{sn}}\frac{\mu_n\sin(\omega\tau/2)\sin(\lambda_n b)}{\lambda_n^2\left[2\mu_n h+\sin(2\mu_n h)\right]}\mathrm{e}^{-\lambda_n x}\sin\left(\omega t-\frac{\omega\tau}{2}\right)\mathrm{d}\omega\Bigg\}.\end{aligned} \tag{3.14}$$

4 Approximation for large x

For $x/h >> 1$, the contribution of the evanescent modes, given in the third line of (3.13), is negligible. When the method of stationary phase to the propagating modes is applied, the first and second lines in (3.13) give for the free surface:

$$\begin{aligned}\hat{\eta}=&\frac{2^{7/4}\sin\left[\sqrt{2}\hat{\tau}\left(\hat{t}/\hat{x}-1\right)^{1/2}/2\right]\sin\left[\sqrt{2}\hat{b}\left(\hat{t}/\hat{x}-1\right)^{1/2}\right]\cosh\left[\sqrt{2}\left(\hat{t}/\hat{x}-1\right)^{1/2}\right]}{\sqrt{\pi}\hat{\tau}\hat{x}^{1/2}\left(\hat{t}/\hat{x}-1\right)^{3/4}\left\{2^{3/2}\left(\hat{t}/\hat{x}-1\right)^{1/2}+\sinh\left[2^{3/2}\left(\hat{t}/\hat{x}-1\right)^{1/2}\right]\right\}}\cos\left[\sqrt{2}\hat{x}\left(\hat{t}/\hat{x}-1\right)^{3/2}-\frac{\pi}{4}\right]\\&+\sum_{n=1}^{\infty}\frac{(-1)2^{5/2}\hat{t}^{1/2}}{\sqrt{\pi}\alpha_n^{5/2}\hat{c}^{1/2}\hat{\tau}\hat{x}}\left[1-\left(\hat{x}/\hat{c}\hat{t}\right)^2\right]^{5/4}\sin\left[\frac{\alpha_n\hat{c}\hat{\tau}/2}{\sqrt{1-\left(\hat{x}/\hat{c}\hat{t}\right)^2}}\right]\sin\left[\frac{\alpha_n\hat{b}\hat{x}/\left(\hat{c}\hat{t}\right)}{\sqrt{1-\left(\hat{x}/\hat{c}\hat{t}\right)^2}}\right]\\&\times\cos\left[\alpha_n\left(\hat{c}^2\hat{t}^2-\hat{x}^2\right)^{1/2}+\frac{\pi}{4}\right].\end{aligned} \tag{4.1}$$

The first line in (4.1) represents the tsunami, and is valid[2] for $1.2\hat{x} > \hat{t} > \hat{x}$. The terms under the sum represent acoustic-gravity modes, and become valid (see footnote 2) for any $\hat{t} \geq \hat{x}/\hat{c}$. All variables in (4.1) are made dimensionless, according to:

$$\hat{\eta}=\eta/\tilde{\zeta}_o,\ \hat{x}=x/h,\ \hat{b}=b/h,\ \hat{t}=\tilde{t}-0.5\hat{\tau},\ \tilde{t}=t\sqrt{g/h},\ \hat{\tau}=\tau\sqrt{g/h},\ \hat{c}=c/\sqrt{gh}.$$

Similarly, (3.14) gives for the bottom pressure:

$$\begin{aligned}\hat{P}_b\equiv\frac{P_b}{\rho g\tilde{\zeta}_o}=&\frac{2^{7/4}\sin\left[\sqrt{2}\hat{\tau}\left(\hat{t}/\hat{x}-1\right)^{1/2}/2\right]\sin\left[\sqrt{2}\hat{b}\left(\hat{t}/\hat{x}-1\right)^{1/2}\right]\cos\left[\sqrt{2}\hat{x}\left(\hat{t}/\hat{x}-1\right)^{3/2}-\frac{\pi}{4}\right]}{\sqrt{\pi}\hat{\tau}\hat{x}^{1/2}\left(\hat{t}/\hat{x}-1\right)^{3/4}\left\{2^{3/2}\left(\hat{t}/\hat{x}-1\right)^{1/2}+\sinh\left[2^{3/2}\left(\hat{t}/\hat{x}-1\right)^{1/2}\right]\right\}}\\&+\sum_{n=1}^{\infty}\frac{2^{5/2}\hat{t}^{1/2}\hat{c}^{3/2}}{\sqrt{\pi}\alpha_n^{3/2}\hat{\tau}\hat{x}}\left[1-\left(\hat{x}/\hat{c}\hat{t}\right)^2\right]^{1/4}\sin\left[\frac{\alpha_n\hat{c}\hat{\tau}/2}{\sqrt{1-\left(\hat{x}/\hat{c}\hat{t}\right)^2}}\right]\sin\left[\frac{\alpha_n\hat{b}\hat{x}/\left(\hat{c}\hat{t}\right)}{\sqrt{1-\left(\hat{x}/\hat{c}\hat{t}\right)^2}}\right]\\&\times\cos\left[\alpha_n\left(\hat{c}^2\hat{t}^2-\hat{x}^2\right)^{1/2}+\frac{\pi}{4}\right]\end{aligned} \tag{4.2}$$

[2] These constraints result from the limitations of the method of stationary phase and from the approximations made in calculating the stationary points.

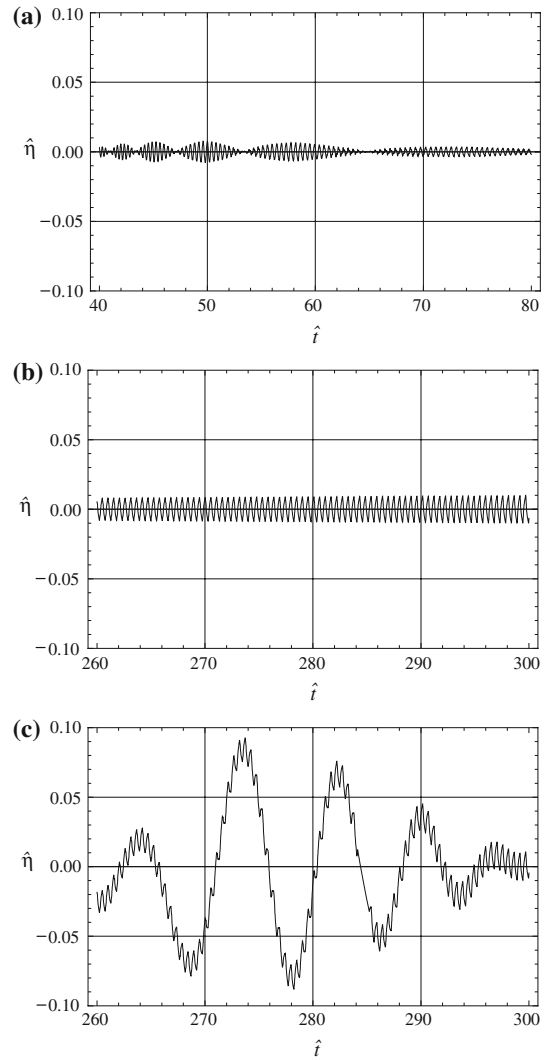

Fig. 3 Temporal evolution of the free-surface at $\hat{x} = 250$, and $n = 10$. **a** Arrival of *Acoustic-Gravity* waves, **b** *Acoustic-Gravity* waves for $t \in (5200\,\text{s}, 6000\,\text{s})$, **c** *Acoustic-Gravity* wave together with tsunami for $t \in (5200\,\text{s}, 6000\,\text{s})$

Note that the frequencies (i.e., the stationary points) and wave-numbers of the tsunami and of the acoustic-gravity waves are approximately

$$\hat{\omega}_o = \omega_o h^{1/2}/g^{1/2} = \sqrt{2}\left(\hat{t}/\hat{x} - 1\right)^{1/2}, \quad \hat{k}_o = hk_o = \hat{\omega}_o, \tag{4.3a,b}$$

and

$$\hat{\omega}_n = \omega_n h^{1/2}/g^{1/2} = \frac{\alpha_n \hat{c}}{\sqrt{1 - \left(\hat{x}/\hat{c}\hat{t}\right)^2}}, \ \hat{k}_n = hk_n = \frac{\alpha_n \left(\hat{x}/\hat{c}\hat{t}\right)}{\sqrt{1 - \left(\hat{x}/\hat{c}\hat{t}\right)^2}}, \quad n = 1, 2, \ldots. \tag{4.4a,b}$$

The leading-order approximations for the group velocities of the tsunami and the acoustic-gravity waves are:

$$\hat{c}_{g_o} = c_{g_o}/h^{1/2}g^{1/2} = 1, \quad \text{for } 1.2\hat{x} > \hat{t} > \hat{x}, \tag{4.5a}$$
$$\hat{c}_{g_n} = c_{g_n}/h^{1/2}g^{1/2} = \hat{x}/\hat{t}, \quad \text{for any } \hat{t} \geq \hat{x}/\hat{c}. \tag{4.5b}$$

5 Example

In order to assess the physical magnitude of the *Acoustic-Gravity* wave phenomenon, the following example is chosen:

gravity	$g = 10\,\mathrm{m/s^2}$
speed of sound	$c = 1500\,\mathrm{m/s}, \quad \hat{c} = 7.5$
water depth	$h = 4000\,\mathrm{m}$
lateral extent of bottom motion	$b = 40000\,\mathrm{m}, \quad \hat{b} = 10$
vertical extent of bottom motion	$\tilde{\zeta}_o = 1\,\mathrm{m}$
duration of bottom motion	$\tau = 10\,\mathrm{s}, \quad \hat{\tau} = 0.5$
distance of observation point	$x = 1{,}000{,}000\,\mathrm{m}, \quad \hat{x} = 250.$

For this example, the *Acoustic-Gravity* waves arrive at the observation point at $t_{\mathrm{a.g}} \approx 667\,s$, whereas the tsunami reaches this point at $t_{\mathrm{ts}} \approx 5000\,s$, leaving an option for an advance warning of more than an hour.

The variations of the free-surface elevation, and of the dynamic bottom pressure, as functions of time, are given in Figs. 3 and 4, respectively, for two time intervals: $t \in (800\,\mathrm{s}, 1600\,\mathrm{s})$, and $t \in (5200\,\mathrm{s}, 6000\,\mathrm{s})$; corresponding to $\hat{\tau} \in (40, 80)$, and $\hat{\tau} \in (260, 300)$, respectively.

From Fig. 3, one can see that the amplitude and period of the *Acoustic-Gravity* wave are about 0.01 m and 10 s, respectively. These waves have a wave-length of about 40 km. The feasibility to distinguish these waves from

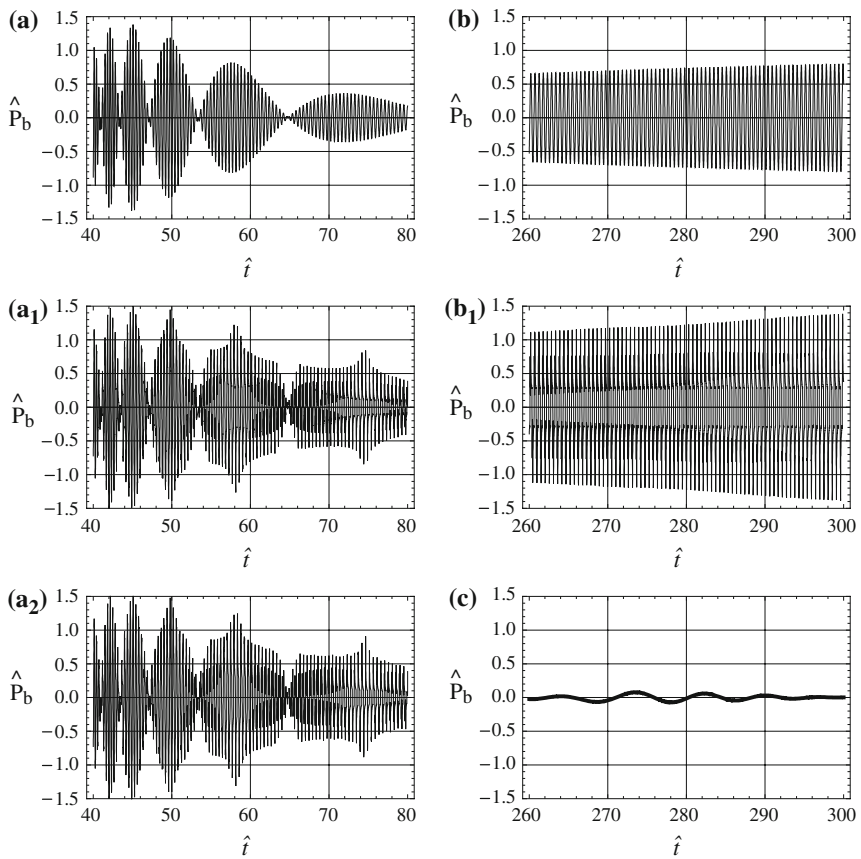

Fig. 4 Temporal evolution of the dynamic bottom pressure at $\hat{x} = 250$; for two different time intervals and three different numbers of *Acoustic-Gravity* modes. **a** $t \in (800\,\mathrm{s}, 1600\,\mathrm{s})$, $n = 1$. $\mathbf{a}_1$ $t \in (800\,\mathrm{s}, 1600\,\mathrm{s})$, $n = 10$. $\mathbf{a}_2$ $t \in (800\,\mathrm{s}, 1600\,\mathrm{s})$, $n = 100$. **b** $t \in (5200\,\mathrm{s}, 6000\,\mathrm{s})$, $n = 1$. $\mathbf{b}_1$ $t \in (5200\,\mathrm{s}, 6000\,\mathrm{s})$, $n = 10$. **c** $t \in (5200\,\mathrm{s}, 6000\,\mathrm{s})$, tsunami only

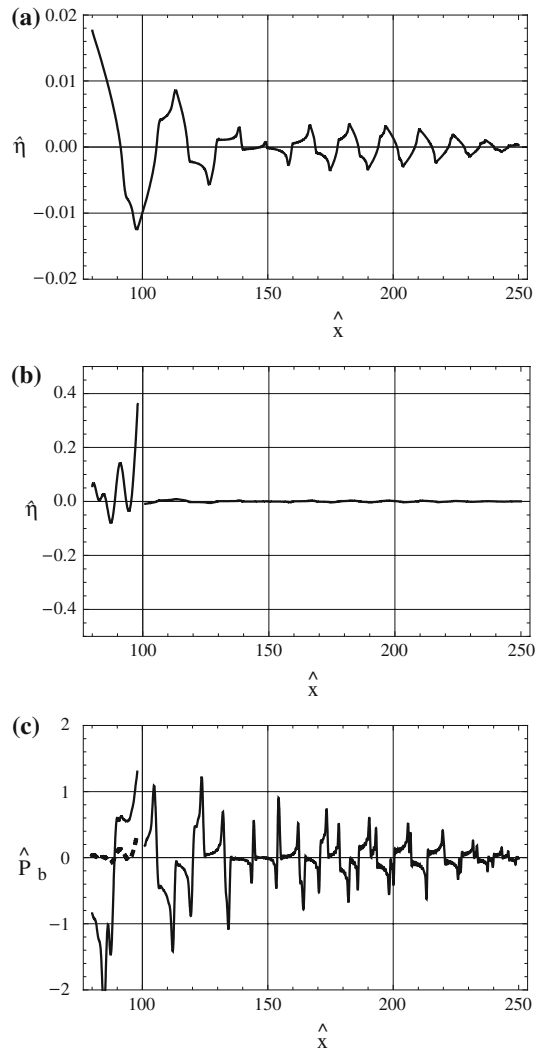

Fig. 5 Spatial evolution for $\hat{t} = 100$ ($t = 2000$ s), for $x \in (320{,}000\,\text{m}, 10^6\,\text{m})$, $n = 10$. **a** Free-surface elevation, acoustic waves only, **b** free-surface elevation, tsunami together with acoustic-gravity waves, **c** bottom pressure; *solid line* acoustic-gravity waves only; *dashed line* tsunami only

prevailing wind-waves using surface measurements, is rather doubtful. However, from Fig. 4 one can see that these *Acoustic-Gravity* waves cause significant fluctuations in the bottom-pressure, with the same period of 10 s and amplitude of one tenth of an atmosphere. Thus, the bottom pressure seems to be a much better 'candidate' for field measurements, and early warning against the tsunami.

Figure 3c gives the *Acoustic-Gravity* waves superposed on the tsunami. In our example, the amplitude and period of the tsunami are about 0.1 m and 200 s, respectively. The wave-length is of the order of 40 km.

From Fig. 4c one can see the minute effect of the tsunami on the bottom pressure, in particular in comparison to that of the *Acoustic-Gravity* waves. Comparing Fig. 4a, $4a_1$, and $4a_2$ demonstrates that a reasonable choice for the number of terms in the series of Eqs.4.1 and 4.2 is $n = 10$ or so.

The spatial variation of the free-surface and the bottom pressure are given in Fig. 5 for $t = 2000$ s, and $x > 320$ km. Note that gaps were left in Fig. 5b and c for $\hat{x} \in (98, 101)$. These gaps result from the fact that the method of stationary phase fails at the front of the tsunami; see [10].

6 Concluding remarks

The aim of this paper has been to bring forward the possibility to utilize measurements of *Acoustic-Gravity* waves as precursors to tsunamis. To accomplish such a task one would have to solve an inverse problem. This seems to be an achievable task when analytical solutions like the one presented in this paper are available.

Note that the first few acoustic-gravity modes have wave lengths that significantly exceed the width of the underwater sound channel (SOFAR), [11,12], and consequently cannot be trapped in it. For them, the whole depth of the ocean serves as a waveguide.

In conclusion, it is important to mention that the effects of energy dissipation by bottom friction, and of energy scattering by bottom irregularities, have been neglected in this study. Moreover, more realistic estimates require bottom elasticity to be taken into account. These, as well as three-dimensional effects, may act to reduce the chances to detect acoustic-gravity waves far from the epicenter.

A study which applies the method of separation of variables to the wave equation and the linearized free-surface boundary conditions in elliptic cylindrical coordinates is currently being carried out. This study is expected to provide analytic solutions in terms of series of Mathieu functions for the three-dimensional problem.

Acknowledgements This research was supported by the US-Israel Binational Science Foundation (Grant 2004-205), and by the Israel Science Foundation (Grant 63/09). The technical assistance and helpful discussions with Dr. Amir Regev and Dr. Y. Toledo, are much appreciated.

References

1. Nosov MA (1999) Tsunami generation in compressible ocean. Phys Chem Earth B 5:437–441
2. Nosov MA (2000) Tsunami generation in a compressible ocean by vertical bottom motions. Izv Atmos Ocean Phys 36:661–669
3. Nosov MA, Skachko SM (2001) Nonlinear tsunami generation mechanism. Nat Hazards Earth Syst Sci 1:251–253
4. Nosov MA, Kolesov SV, Ostroukhova AV, Alekseev AB, Levin BW (2005) Elastic oscillations of the water layer in a tsunami source. Doklady Earth Sci 404(7):1097–1100
5. Nosov MA, Kolesov SV (2007) Elastic oscillations of water column in 2003 Tokachi-oki tsunami source: in-situ measurements and 3-D numerical modeling. Nat Hazards Earth Syst Sci 1:243–249
6. Miyoshi H (1954) Generation of the tsunami in compressible water (Part I). J Oceanogr Soc Jpn 10:1–9
7. Sells CCL (1965) The effect of a sudden change in shape of the bottom of a slightly compressible ocean. Phil Trans R Soc Lond A 1092:495–528
8. Yamamoto T (1982) Gravity waves and acoustic waves generated by submarine earthquakes. Soil dyn Earthq Eng 1:75–82
9. Ohmachi T, Tsukiyama H, Matsumoto H (2001) Simulation of tsunami induced by dynamic displacement of seabed due to seismic faulting. Bull Seism Soc Am 91:1889–1909
10. Berry MV (2005) Tsunami asymptotics. N J Phys 7, article number 129, 18 pp
11. Okal EA, Talandier J (1986) T-wave duration, magnitudes and seismic moment of an earthquake; application to tsunami warning. J Phys Earth 34:19–42
12. Okal EA, Alasset P-J, Hyvernaud O, Schindelé F (2003) The deficient T waves of tsunami earthquakes. Geophys J Int 152(2):416–432